Supporting Information for

A fast, single-vesicle fusion assay mimics physiological SNARE requirements.

Erdem Karatekin[1,4,*], Jérôme Di Giovanni[2,3], Cécile Iborra[2,3], Jeff Coleman[4]
Ben O'Shaughnessy[5], Michael Seagar[2,3], & James E. Rothman[4,*]

[1]*Laboratoire de Dynamique membranaire, CNRS FRE 3146, IBPC, 13 rue Pierre et Marie Curie 75005 Paris, France.* [2]*Institut National de la Santé et de la Recherche Médicale, Unité 641, Bd P. Dramard, Marseille F-13000 France.* [3]*Université de la Mediterranée-Aix Marseille 2, Faculté de Médecine Secteur Nord, Bd P. Dramard, Marseille F-13000, France* [4]*Yale University, School of Medicine, Department of Cell Biology, 333 Cedar Street New Haven, CT 06520.* [5]*Department of Chemical Engineering, Columbia University, New York, New York 10027.*

[*] To whom correspondence should be addressed

E-mail: erdem.karatekin@yale.edu, james.rothman@yale.edu

Materials and Methods

Recombinant protein expression and purification. Either recombinant Syb2-His_6 (from plasmid pTW2 (*1*)), or a Syb2-spacer-myc-His_6 (in a p28a vector, ref. 2) was used, without any noticeable difference in results. Syb2-His_6 was expressed and purified as described (*1*). The spacer in the second construct consists of 13 amino acids (KGVEPKTYCYYSS (*2*)). *E. coli (Rosetta2 (DE3),* Novagen) was transformed with the second plasmid and grown to $OD_{600\,nm}$

=0.7 in Luria Bertani (LB) medium at 37°C, and then induced with 0.5 mM IPTG. Bacteria were pelleted using centrifugation at 4500 rpm for 15 min in a JLA16.250 rotor (Beckman Coulter Avanti J-E centrifuge) and resuspended in MCAC buffer (20 mM Tris-HCl, 1.5% CHAPS, 500 mM NaCl, 20 mM imidazole, 10% glycerol, protease inhibitors, pH=8.0) before lysis using a French Press. Debris were eliminated by centrifugation at 13,000x g for 30 min in an Eppendorf centrifuge and the supernatant was incubated with Ni-NTA-agarose beads (Qiagen). Beads were loaded onto a column and washed with MCAC buffer containing 0.6% CHAPS and 50 mM imidazole. Recombinant Syb2 was eluted using 500 mM imidazole in the same buffer.

Soluble Syb2$_{1-92}$ (amino acids 1-92) was expressed in *Rosetta2 (DE3)* cells as for Syb2-spacer-myc-His$_6$. The bacterial pellet was resuspended in TBS buffer (50 mM Tris HCl, 150 mM NaCl, 20 mM imidazole, 1% Triton X100, protease inhibitors, pH 8) and lysed in a French press. The supernatant was incubated with Ni-NTA-agarose beads (Qiagen) which were then loaded onto a column and washed with TBS (pH=7) containing 50 mM imidazole. Recombinant protein was eluted using 500 mM imidazole and dialysed overnight at 4 °Cin 25 mm Hepes-NaOH, 140 mM KCl, 1 mM DTT, pH=7.4.

To purify the t-SNARE acceptor complex, we used two strategies. In the first, *E. coli* (*Rosetta2 (DE3)*, Novagen) was co-transformed with a pGEX-KG vector containing N-terminally GST-tagged rat Syx1A and a pET28 vector containing N-terminally 6xHis tagged rat SNAP25. Culture and purification conditions were similar to the protocol for Syb2 above, except a dual step purification using both GST and 6xHis tags were used to select for intact complex. First, SNAP25•Syx complexes and free SNAP25 were isolated on a Ni-agarose column (Amersham Bioscience). After elution with imidazole, SNAP25•Syx was purified using a glutathione-Sepharose column (Amersham Bioscience), i.e. free SNAP25 was eliminated by extensive washing with PBS (pH=8) containing 0.3% sodium cholate. The GST tag on Syx was cleaved using 100 u/ml thrombin (2 hrs, 37 °C) to release the heterodimer from the beads. In the second

approach, a polycistronic vector coding rSyx1A (no tag) and His_6-mSNAP25 was used (plasmid pTW34). Expression and purification were as described in Parlati *et al.* (*3*).

Recombinant mSNAP25B bearing an N-terminal GST tag and a PreScission protease site (plasmid pJM46) was transformed into *E. coli Rosetta 2* (*DE3*) cells. After cell lysis, GST-SNAP25B was isolated on a column packed with Glutathione Sepharose 4B beads (GE Healtcare), and eluted using *in situ* cleavage by PreScission protease (GE Healtcare) following the manufacturer's instructions.

Recombinant rSyx-1A bearing an N-terminal 6xHis-SUMO tag (a kind gift of Jingshi Shen, Dept. of Molecular, Cellular, and Developmental Biology, U. of Colorado) was expressed and purified as other recombinant proteins, except an AKTA prime system (GE Healthcare) running a 50-500 mM imidazole gradient was used to elute the protein. Purified His_6-SUMO-Syx1A was cleaved with SUMO protease during dialysis overnight at $4\,^{\circ}\mathrm{C}$. The His_6-SUMO tag was removed using a Ni-NTA column.

A plasmid coding for TeNT light chain (in a pQE-3 vector) was used to transform *E. coli JM109* bacteria cultured in 2YT medium. The recombinant protein was purified on a Ni-NTA column as described (*2*).

Preparation of SUVs and SBLs. SNARE proteins were reconstituted into liposomes essentially as described with small differences (*4*). All lipids were from Avanti Polar Lipids (Alabaster, AL), and were dissolved in a 2:1 v/v mixture of $CHCl_3$:methanol. Typically, 1 μM total lipid was used, with a composition that was 78 mole % 1,2-dioleoyl-*sn*-glycero-3-phosphocholine (DOPC), 15 mole % 1,2-dioleoyl-*sn*-glycero-3-phospho-L-serine (DOPS), 5 mole % 1,2-dioleoyl-*sn*-glycero-3-phosphoethanolamine-N-[methoxy(polyethylene glycol)-2000] (PEG2000-PE), and 2 mole % fluorescently labeled lipids, either 1,2-dioleoyl-*sn*-glycero-3-phosphoethanolamine-N-(7-nitro-2-1,3-benzoxadiazol-4-yl) (NBD-PE), or 1,2-dioleoyl-*sn*-

glycero-3-phosphoethanolamine-N-(lissamine rhodamine B sulfonyl) (LR-PE). Lipids were first dried either in a rotavap or under a nitrogen stream and then were kept under high vacuum for at least 2 hrs to remove traces of organic solvent. Dried lipids were re-hydrated in reconstitution buffer (RB, 25 mM HEPES, 140 mM KCl, and 0.2 mM TCEP or 0.25 mM DTT, pH=7.4) with the desired amount of protein and a total of 1.5% (v/w) n-octyl-β-D-glucoside (OG) or 0.8% (v/w) sodium cholate. The mixtures were shaken vigorously, diluted 4 times to 2 ml using RB, then dialyzed overnight against 5 l of RB supplemented with 5 g SM-2 Biobeads (Bio-Rad) using Spectra-Por biotechnology grade regenerated cellulose dialysis bags with a molecular weight cutoff of 3,500 Da. Dialyzed samples were mixed 1:1 (v/v) with 60% iodoxanol (Optiprep, Axis-Shield PoC, Oslo,Norway) and layered below 20% and 0% iodoxanol in RB. After centrifugation in a Beckman SW41 Ti rotor at 38,000 rpm, 4-5 hr at 4^{o}C, 400-500 μl of liposomes were harvested at the 0%-20% interface. Some reconstitutions and fusion tests were made in the presence of 1 mM EGTA to remove calcium. Results from such experiments were indistinguishable from results obtained when EGTA was omitted.

SBLs were formed by incubating protein-free (pf) or t-SUVs over very hydrophilic #1.5 glass coverslips (Waldemar Knittel Glasbearbeitungs-GmbH, Braunschweig, Germany), which were prepared by, in sequence, cleaning in a hot Hellmanex II solution, extensive rinsing with MQ water, Piranha cleaning (a 2:1 mixture of sulfuric acid and hydrogen peroxide), extensive rinsing with MQ water, drying and plasma cleaning (Harrick PDC-32G Plasma Cleaner/Sterilizer, Harrick Plasma, Ithaca, NY). A clean coverslip was bonded with a an elastomer block made of poly(dimethyl siloxane) (PDMS) containing microfabricated grooves which formed flow channels (Fig. 1). When a solution of SUVs is introduced, the SUVs first adsorb onto the glass coverslip, then burst and fuse to form supported bilayers during the 45-60 min incubation time (*5*). After extensive rinsing with buffer and for every SBL we formed, we checked the homogeneity of the SBL down to the diffraction limit using the NBD-labeled lipids included in the bilayers.

Then the fluidity of the SBL was verified by fluorescence recovery after photobleaching (FRAP, a sample trace is shown in Fig. S2). Only if a SBL passed these quality checks did we introduce a solution of v-SUVs into the channel, at a typical concentration of 40-60 nM lipid. Given that the mean vesicle diameter is ~ 50 nm (see below), and assuming 0.7 nm^2 per lipid (*6*), this corresponds to 2-3 pM SUV. Typically, pf- or v-SUVs were diluted $(2-5)\times 10^5$ times before use.

Quantification of actual L:P ratios. Actual lipid-to-protein ratios were obtained using a combination of densitometry for quantifying protein concentrations and fluorescence for lipids.

For lipid quantification, calibration curves were constructed by measuring the fluorescence from known concentrations of NBD-PE and LR-PE lipids dissolved in a $CHCl_3$:MeOH 2:1 v/v mixture. The calibration curve for NBD-PE is shown in fig. S1c. For quantifying SUV yields, a 5 μl SUV sample was dissolved in 995 μl $CHCl_3$:MeOH 2:1 v/v mixture. This solution was placed in a 2 mm $\times$ 10 mm quartz fluorescence cuvette (Hellma GmbH & Co. KG, Germany) and its fluorescence was measured in a Perkin Elmer LS-55 fluorescence spectrometer using $\lambda_{ex} = 472$ nm and $\lambda_{em} = 530$ nm for NBD-PE and $\lambda_{ex} = 560$ nm and $\lambda_{em} = 577$ nm for LR-PE (10 nm slits). The measured fluorescence values were converted to lipid concentrations using the calibration curves.

For quantifying protein yield, various known concentrations of purified Syb or the t-SNARE complex SNAP25•Syx1 were loaded onto a Novex Bis-tris SDS minigel. In parallel, some of the lanes of the gel were loaded with t- or v-SUVs of known lipid concentration and nominal L:P ratios. For protein concentrations that were sufficiently high, we used coomassie staining (fig. S1b). The stained gel was scanned, and the intensities of the bands quantified using the "Gels" function of ImageJ software (Wayne Rasband, National Institutes of Health). The bands with known concentrations of protein were used to construct a calibration curve against which

the concentrations of the unknown samples were tested. For samples with low protein content, immunoblotting was used (fig. S1a), with monoclonal antibodies against Syb (CL69.1) or Syx (HPC1). Chemiluminescence from an anti-mouse IgG, HRP-linked secondary antibody (Cell Signaling Tech.) was generated using the Bio-Rad Chemiluminescence kit ECL for HRP and recorded on photographic film. After digitizing the photographic film (shown on the left, fig. S1a), densitometry analysis was carried out as for Coomassie stained samples.

The protein and lipid yields coincided to within measurement error. Therefore, the nominal and the actual L:P ratios are the same.

Characterization of the SUVs by dynamic light scattering (DLS). All measurements were made at the Keck Foundation Biotechnology Resource Laboratory at Yale University using a Wyatt Technology DynaPro instrument (Wyatt Technology Corporation, Santa Barbara, CA) at 90 ° configuration at 20-25% laser power and 25 °C. Liposome stock solutions were diluted $100\times$ in RB and placed in a Hellma 30 μl DLS cell. For every sample, 30 acquisitions, each lasting 10 s, were averaged. Intensity autocorrelations, $g_2(\tau)$, were recorded for delays between 0.5 μs and 7.3×10^6 μs and analyzed using a cumulant expansion reformulated using moments about the mean decay rate, $\overline{\nu}$, (*7*):

$$g_2 = B + \beta e^{-2\overline{\nu}\tau}\left(1 + \frac{\mu_2}{2!}\tau^2 - \frac{\mu_3}{3!}\tau^3 \cdots\right)^2 , \qquad (1)$$

where B is the baseline (ideally $= 1$), β is a factor that depends on experimental geometry, $\mu_m \equiv \int_0^\infty \mathrm{d}\nu\, G(\nu)(\nu - \overline{\nu})^m$ is the m'th moment about the mean, and $G(\nu)$ is the distribution of relaxation rates. The mean, variance and skewness correspond to $m = 1, 2,$ and 3, respectively. The decay rate is related to the diffusion coefficient, D, by $\overline{\nu} = Dq^2$, where $q = (4\pi n/\lambda_0)\sin(\theta/2)$ is the magnitude of the scattering wavevector, $n = 1.340$ is the refractive index of the medium, $\lambda_0 = 828$ nm is the incident light wavelength in vacuum, $\eta = 1.019$ mN.s/m^2 is the viscosity of the medium, and $\theta = \pi/2$ is the scattering angle. After fitting eq.

(1) to experimental autocorrelations (Fig. S3), the Stokes-Einstein relation, $D = \mathrm{kT}/(6\pi\eta\overline{R}_h)$, is used to obtain the mean hydrodynamic radius, $\overline{R}_h$, which is converted to the number-averaged radius, $\overline{R}_n$, using $\overline{R}_n \approx \overline{R}_h/(1+3\delta_z)$, where $\delta_z \equiv (\langle\nu^2\rangle - \langle\nu\rangle^2)/\langle\nu\rangle^2 = \mu_2/\overline{\nu}^2$ is the relative variance of the distribution of the relaxation rates, valid if skewness is negligible (*8*). The advantage of this method over other cumulant expansions is the insensitivity of the best fit parameters to the cutoffs chosen for delays. A typical autocorrelation measurement and the corresponding fit are shown in fig. S3. Averaging 26 measurements yielded $\overline{R}_n = 29 \pm 1.5$ nm ($\pm$ s.e.m.) and relative variance $\delta = 0.48$. This value includes the ~ 4 nm thick PEG brush; thus, the average bare SUV radius is ~ 25 nm, which is the value used to convert lipid concentrations to SUV concentrations and to calculate the number of proteins per vesicle from the lipid:protein ratios, and is in close agreement with previous independent measurements by electron microscopy (*4*).

Microfluidic flow channels. Elastomer blocks with grooves were produced by cross linking poly-(dimethyl siloxane) (PDMS, Sylgard 184 silicone elastomer kit, Dow Corning, Midland, MI) poured over a SU-8 (MicroChem Corp., Newton, MA) template fabricated using standard photolithography at the class 100 cleanroom at the Center for Microelectronic Materials and Structures (μELM) at Yale University. Photolithographic masks for producing templates were also made at the Yale μELM cleanroom. Channels were $300 - 500$ μm wide, $50 - 80$ μm high, and ~ 2 cm long and were connected to a reservoir and a syringe pump (either a model KDS210 from KdS Scientific Inc., Holliston, MA or a model F200 from Chemyx Inc., Houston, TX) using poly(tetrafluoroethylene) tubing. Some templates, used in Paris at the early stages of this study, were a kind gift from Rafaele Attia and Jean-Louis Viovy, Institut Curie, Physico-Chimie Curie, CNRS UMR 168, Paris.

Microscopy and analysis of fusion events. Either an Olympus IX 71 or a Nikon Ti Eclipse inverted microscope was used. The Olympus microscope was equipped with an Olympus UP-

LAPO 100XOI3PH 100×/1.35 oil immersion objective, a high pressure mercury arc lamp, a heated microscope stage for temperature control and a SensiCam LE VGA CCD camera (PCO AG, Kelheim, Germany). The Nikon microscope had a 60×/1.45 oil objective, a metal halide lamp, an Air-Therm (World Precision Instruments, Sarasota, FL) temperature controller, and an Andor iXon DU897E EM-CCD (512×512 pixels). Filter sets for NBD ($\lambda_{ex} = 460 - 490$ nm, $\lambda_{em} = 515 - 550$ nm) and for Lissamine-Rhodamine ($\lambda_{ex} = 532.5 - 557.5$ nm, $\lambda_{em} = 570 - 640$ nm, Chroma ET-Cy3 set) were from Chroma Technology Corp., Rockingham, VT. Streams were acquired typically at a rate of 10 images/s for 500-1000 frames. Docking and fusion events were marked manually by clicking on vesicles using the PointPicker plugin (Philippe Thévenaz, Biomedical Imaging Group, Swiss Federal Institute of Technology, Lausanne) of ImageJ which records the $x, y,$ and frame coordinates of every click into a text file (http://bigwww.epfl.ch/thevenaz/pointpicker/). For definitions of the docking and fusion frames and an example, see fig. 1 in the main text. The PointPicker information was used to calculate the cumulative fusion rates and delays between individual docking and fusion events using MatLab (The MathWorks, Natick, MA). The unnormalized fusion rate, $\dot{F}$, was calculated by fitting a straight line passing through the origin to the cumulative fusions as a function of time (fig. 2a), provided the total number of fusions in a given movie was > 10. Otherwise, $\dot{F}$ was calculated as the total number of fusions in a movie, divided by its duration. Fusion rates were normalized by the measurement area in μm^2 and pM SUV concentration, assuming 2×10^4 lipids per SUV.

Empirical distributions of the delays between individual docking and fusion events were calculated either as a probability density function (PDF, the probability that fusion occurred between delay τ and $\tau+\Delta\tau$, where $\Delta\tau$ is the bin width) or a survivor function (SF, probability that fusion occurred at delay $> \tau$). In fig. S11a-d, the theoretical PDFs for the SNARE recruitment model (see below) are plotted together with the experimental data. For fig. S11e,f, we used a

non-linear least squares fitting routine (the "lsqcurvefit" function of the Optimization Toolbox of MatLab), and used the χ^2 value to assess the goodness of fits. For these analyses, delays > 0.8 s were ignored ($\leq 15-20$% of delays), as longer delays seem to be due to non-specific fusions (see the section *Long tail of the delay distributions*).

For the experimental SFs in fig. S5, best fit parameters to a mixture of two exponential distributions of the form $a\ \exp(-t/\tau_1) + (1-a)\ \exp(-t/\tau_2)$, were obtained using a maximum likelihood estimation (MLE) using the Statistics Toolbox of MatLab. All delays were taken into account.

To fit 2-dimensional Gaussian functions to fluorescence intensity profiles of fusing vesicles as in fig.1, a non-linear least squares fitting algorithm was used (the "lsqcurvefit" function of the Optimization Toolbox of MatLab). Our approach was originally inspired from the Wiseman group's image correlation spectroscopy algorithms (http://wiseman-group.mcgill.ca).

Effect of excitation light intensity. We did not detect significant changes to the distribution of delay times when the light intensity was varied (Supplementary Fig. 4), indicating fusion is not driven by light under our experimental circumstances.

Long tail of the delay distributions

Although $75-85$ % of delays between docking and fusion were ≤ 0.8 s, a slowly fusing population is evident in the delay distributions (Fig. 3b), as previously described by the Weisshaar group (*9*). To gain insight into the origin of the long time-scale, we compared distributions of delays between docking and fusion between v-SUVs and either t- or protein-free (pf)-SBLs in experiments run in parallel. For delays obtained using t-SBLs, we used a mixture of exponential distributions to estimate the characteristic time of the slow component. An exponential fit does not capture the short time scale behaviour since a peak is invariably present in the probability

densities at short delays (see main text), but here we are solely concerned with the long time behaviour. Delays for v-SUV/pf-SBL fusions are well fit by a single exponential distribution with the same time scale as the slow decay time τ_2 from v-SUV/t-SBL experiments run in parallel (Supplementary Fig. 5), even though fusion events are rare and therefore fits are less reliable. When we attempted to fit a mixture of two exponentials to the v-SUV/pf-SBL data, essentially a single component with time scale $\approx \tau_2$ was obtained. This suggests that the long time scale is due to non-specific interactions between v-SUVs and SBLs, whether or not the latter contain t-SNAREs, despite the use of a protective PEG brush. Syb has a series of basic residues in its juxtamembrane domain that can interact with acidic lipids in apposed bilayers in *trans* (*2*). Alternatively, defects in the SBL or impurities may provide rare docking opportunities. When docked for a sufficiently long time, a SUV may fuse with a SBL in a non-specific manner. The presence of t-SNAREs in the SBL is expected to enhance this non-specific fusion, by providing more opportunities for docking. Liu *et al.* (*9*) and Domanska *et al.* (*10*) also reported a long time scale, which they did not examine.

Delays between docking and fusion are limited by recruitment of t-SNAREs

We examined delay distributions as a function of the t-SNARE density on the SBL (at fixed v-SNARE density on the v-SUVs) and N_v, the number of Syb per SUV (at fixed t-SNARE density).

To vary the t-SNARE density, Γ_S, we used either SBLs with nominal t-LP ratios of 10K ($\sim$ 140 t-SNAREs/μm^2) and 30K ($\sim$ 48 t-SNAREs /μm^2), or simply let the v-SUV/t-SBL fusion reactions run for a long time, depleting free t-SNAREs by the formation of SNARE complexes. The former method is direct, but suffers from the drawback that not all t-SNAREs are reconstituted actively into the SBL. This is consistent with previous reports (*9, 11*) and is also evident from the fact that the overall fusion rate increased only by a factor of 1.59 when

the t-SNARE density was increased 3-fold (from t-LP=30K to 10K) and dropped at higher concentrations (fig. S 6). Thus, only a relatively small difference of about 60% in the density of active t-SNAREs is expected between t-LP=30K and 10K SBLs. In the second approach, at early times after introduction of v-SUVs, the t-SNARE density is close to its initial value, whereas as time increases, the t-SNAREs will be depleted. This approach has the advantage that delays from the same SBL and SUV sample are probed, eliminating errors due to experimental variations.

Delay distributions between t-LP=10K and 30K SBLs fusing with v-SUVs (v-LP=150) are shown in fig. 10a. The mean delay for the lower density t-SBLs (t-LP=30K) was longer (200 ms) than that for higher density t-SBLs (t-LP=10K, 180 ms). Another experiment using v-SUVs with v-LP=333 gave a similar result.

A comparison between delays obtained at "early" ($< 1/2$ hr) vs. "late" (> 2 hrs) stages of v-SUV/t-SBL reactions (t-LP=30K, v-LP=150) is shown in fig. S10b. Again, a clear shift to longer delays is observed, with mean delays equal to 200 and 270 ms for early and late stages, respectively. Comparison of early vs. late delays in three other independent comparisons (t-LP=10K/v-LP=150, t-LP=10K/v-LP=333, t-LP=30K/v-LP=333) also yielded longer delays for SBLs with depleted t-SNAREs. Overall, the delays were 183 ± 6 ms for early and 219 ± 20 ms for late delays ($\pm$ s.e.m., n=4).

The fact that in all of the six possible comparisons between the four sets of data, SBLs with depleted t-SNAREs yielded longer delays indicates that delays are limited by how fast t-SNAREs can be recruited to fusion sites.

In sharp contrast, the mean delays are insensitive to the density of v-SNAREs on the SUVs as long as there are enough Syb per SUV to mediate fusion, as shown in fig. 10c. The simplest explanation is that even at the lowest v-SNARE density used ($N_v = 15$), the monolayer density of Syb would be $\rho_v^{min} = (N_v/2)/(4\pi R_{ves}^2) \approx 955$ /μm^2, using $R_{ves} = 25$ nm. Thus, the

minimum v-SNARE areal density is about 7 times larger than the highest density t-SBLs used so that delays are limited by the recruitment of t-, not v-, SNAREs.

These data indicate that pre-formed clusters of t-SNAREs as functional docking/fusion sites can be ruled out, because if all the t-SNAREs needed for fusion were already assembled at the docking/fusion site, delays would remain unchanged when the t-SNARE density was varied (although the overall fusion rate would change).

SNARE recruitment model

The delay times between docking and fusion increased when t-SNARE density was decreased. This observation suggests that fusion requires t-SNAREs to diffuse laterally within the SBL to the docking site; the more dilute the t-SNAREs, the further they must diffuse and hence the greater the delays. Moreover, we have found N^* =5-10 v-SNAREs are required for fusion, suggesting that fusion requires N^* SNAREpins to be formed. Bowen *et al.* (*12*) showed that a single SNAREpin is sufficient for docking. Therefore, forming N^* SNAREpins would require that after docking an additional $p = N^* - 1 =$ 4-9 t-SNAREs be recruited from the SBL to the docking site at which one SNAREpin is already engaged. Now Wagner and Tamm reported that about 57% of t-SNARES were mobile in PEG-cushioned SBLs containing 15% PS as in our experiments (*11*). Thus we assumed the mobile fraction was 0.5, so the effective t-SNARE density in the t-LP=30k SBLs is $\Gamma_s = 24/\mu\text{m}^2$. Thus the required 4-9 t-SNAREs would have to be recruited from a distance $\sim .23 - .35\mu$m, far greater than the radius of the docked SUV. This suggests t-SNAREs must diffuse considerable distances to the docking site before fusion can occur.

Thus motivated, we calculated what the distribution $P(\tau)$ of fusion times τ would be (relative to the instant of docking) assuming only: (i) Active t-SNAREs are homogeneously and randomly distributed about the SBL with mean density Γ_S, (ii) t-SNAREs diffuse independently

in the SBL with diffusion constant D, (iii) a t-SNARE is recruited if ever its diffusion happens to bring it to within the "capture radius" b of the docking site and (iv) fusion occurs when p SNAREs have been cumulatively recruited in this fashion.

The t-SNARE recruitment kinetics in this simple model are essentially those of a planar reaction-diffusion system where the docked vesicle plays the role of a reaction sink of radius b; the mean number of reacted particles after time τ is analogous to the mean number of t-SNAREs recruited a time τ after the docking event, namely $N_s(\tau)$. Thus (*13*)

$$N_s(\tau) = \frac{8\Gamma_S}{\pi} \int_0^\infty \mathrm{d}u \frac{1 - e^{-Du^2\tau}}{u^3 \left\{ \mathrm{J_0}^2(bu) + \mathrm{Y_0}^2 2(bu) \right\}} \,, \tag{2}$$

where J_0 and Y_0 are Bessel functions of the first and second kind, respectively. For times larger than the sink diffusion time, $\tau > t_b \equiv b^2/D$, this expression is well-approximated by a simple form

$$N_s(\tau) \approx \frac{4\pi\Gamma_S D\tau}{\ln(C\tau/t_b)} \,, \tag{3}$$

where $C = 1.274$. Now given the mean number above, the probability that p SNAREs have been recruited after time τ is a Poisson distribution,

$$W(p|\tau) = \frac{N_s^p}{p!} e^{-N_s}. \tag{4}$$

But the probability $F(\tau)$ that p SNAREs have *not yet* been recruited after time τ is the sum of probabilities over all values less than p. This can be written

$$F(\tau) = 1 - \sum_{k=p}^{k=\infty} W(k|\tau) \tag{5}$$

after using the normalization property that the sum over all p values equals unity. Thus the distribution of fusion times is

$$P(\tau) = -\frac{dF}{d\tau} = \frac{N_s^{p-1}}{(p-1)!} \dot{N}_s e^{-N_s} \tag{6}$$

where $N_s(\tau)$ is given by eq. 2 and $\dot{N}_s$ denotes the derivative with respect to τ. The shape of the distribution depends on the value of p, the number of SNAREs which must be recruited.

In fig. 11a,b we compared measured delay time distributions to the predicted distribution of eq. 6 for different values of the parameter p using the simplified form for N_s, eq. 3. For t-SNARE diffusivity we used $D = 0.3$ μm^2/s, the value reported by Wagner and Tamm (*11*) for 15% PS SBLs, while t-SNARE density $\Gamma_S^{30K} = 24$ /μm^2 was used for the t-LP=30K bilayers as discussed above. Though t-LP=10K SBLs carry three times as many t-SNAREs, we found the fusion rate increased by a factor of 1.59 only (Fig. S6), suggesting the density of active t-SNAREs does not scale in proportion to the total t-SNARE density. Thus for t-LP=10K bilayers the effective density of active t-SNAREs relative to the t-LP=30K bilayers was taken to be in proportion to the measured relative fusion rates, giving $\Gamma_S^{10K} = 38$ /μm^2. A value $b = 10$ nm was used for the capture radius.

The same value, $p = 8$, gave best fits to the measured delay time distributions for both t-LP=30K and t-LP=10K bilayers (figs. 11 (a) and (b), respectively). When we instead fixed $p = 8$ and allowed Γ_S to be a variable parameter, for the t-LP=30K bilayers we found best fit model-predicted delay time distributions for densities in the range $\Gamma_S \approx 15 - 25/\mu$m^2 (fig. 11 (c)). This is consistent with our assumed value of $\Gamma_S^{30K} = 24$ /μm^2 based on an assumed 50% active fraction. The model distributions are relatively insensitive to the choice of capture radius b, with best value $b \approx 10$ nm (fig. 11 (d)). Allowing both p and Γ_S to be free fitting parameters, fig. 11(e), returned best values $p = 10$ and $\Gamma_S = 26/\mu$m^2 (t-LP=30K) remarkably consistent with the values above. Finally, the best fit p values exhibited little variation for different values of N_v, the number of SUV v-SNARES, fig. 11(f). The mean over a range of N_v values was $p = 6.9 \pm 3.4$.

Overall, analysis of fusion time distribution data using a simple t-SNARE recruitment model suggests about 4-10 t-SNAREs must be recruited to the docking site for fusion, i.e. a total of

about 5-11 t-SNAREs are required. This is consistent with the 5-10 v-SNARE requirement we established from fusion rate measurements.

References

1. Weber T, et al. (1998) SNAREpins: minimal machinery for membrane fusion. *Cell* 92:759–72.

2. Quetglas S, et al. (2002) Calmodulin and lipid binding to synaptobrevin regulates calcium-dependent exocytosis. *Embo J* 21:3970–9.

3. Parlati F, et al. (1999) Rapid and efficient fusion of phospholipid vesicles by the alpha-helical core of a SNARE complex in the absence of an n-terminal regulatory domain. *Proc Natl Acad Sci U S A* 96:12565–70.

4. Scott BL, et al. (2003) in *Liposomes, Pt B*, Methods in Enzymology (Academic Press Inc, San Diego) Vol. 372, pp 274–300.

5. Schonherr H, Johnson JM, Lenz P, Frank CW, Boxer SG (2004) Vesicle adsorption and lipid bilayer formation on glass studied by atomic force microscopy. *Langmuir* 20:11600–6.

6. Leckband D, Israelachvili J (2001) Intermolecular forces in biology. *Q Rev Biophys* 34:105–267.

7. Frisken BJ (2001) Revisiting the method of cumulants for the analysis of dynamic light-scattering data. *Appl. Optics* 40:4087–4091.

8. Selser JC, Yeh Y (1976) A light scattering method of measuring membrane vesicle number-averaged size and size dispersion. *Biophys. J.* 16:847–848.

9. Liu T, Tucker WC, Bhalla A, Chapman ER, Weisshaar JC (2005) SNARE-driven, 25-millisecond vesicle fusion in vitro. *Biophys J* 89:2458–72.

10. Domanska MK, Kiessling V, Stein A, Fasshauer D, Tamm LK (2009) Single vesicle millisecond fusion kinetics reveals number of SNARE complexes optimal for fast SNARE-mediated membrane fusion. *J Biol Chem* 284:32158–66.

11. Wagner ML, Tamm LK (2001) Reconstituted syntaxin1a/SNAP25 interacts with negatively charged lipids as measured by lateral diffusion in planar supported bilayers. *Biophys J* 81:266–75.

12. Bowen ME, Weninger K, Brunger AT, Chu S (2004) Single molecule observation of liposome-bilayer fusion thermally induced by soluble N-ethyl maleimide sensitive-factor attachment protein receptors (SNAREs). *Biophys J* 87:3569–84.

13. Carslaw HS, Jager JC (1986) *Conduction of heat in solids* (Clarendon Press, Oxford), second edition.

14. Soumpasis DM (1983) Theoretical analysis of fluorescence photobleaching recovery experiments. *Biophys J* 41:95–7.

Supplementary Figures

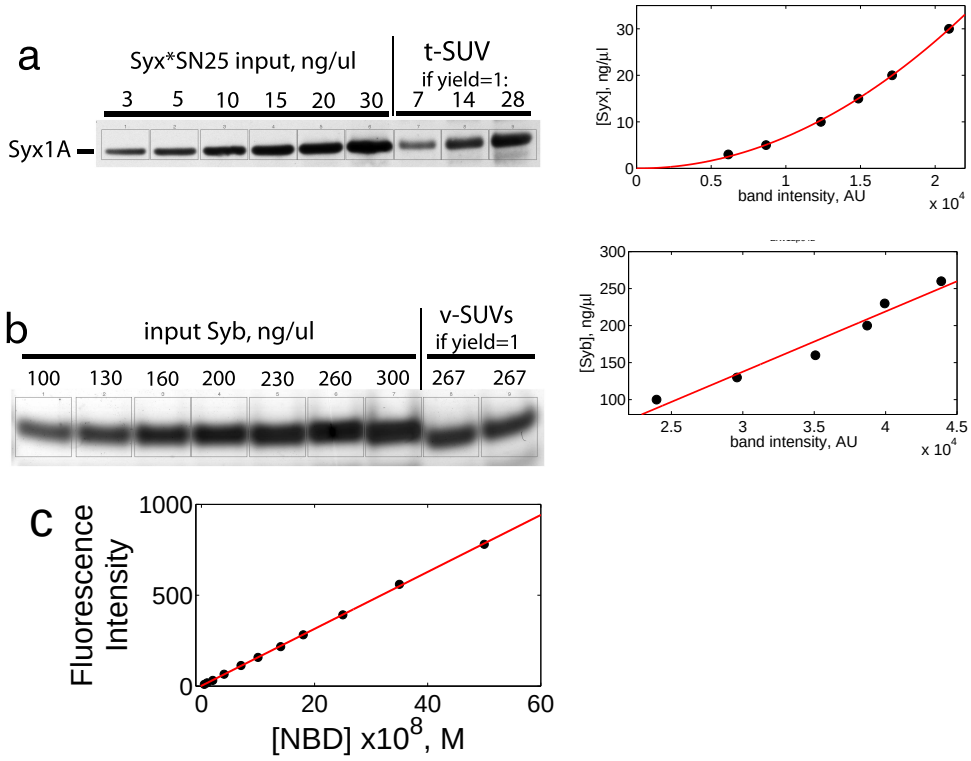

Figure S 1 Quantification of protein and lipid yields after proteoliposome formation. (a) Quantitative western blotting to determine the yield of t-SNAREs reconstituted into SUVs. Left: immunoblot detected on photographic film, and scanned. Lanes 1-6: standards. Lanes 7-9: t-SUVs with nominal t-LP=10K, 5K, 2.5K (10 μl each were loaded) with the indicated protein content if reconstitution yield were 1. Boxes drawn around the bands were used to define intensities using ImageJ (see text). Right: densitometry calibration using the band intensities of protein standards in the left panel. (b) Similar to (a), except Coomassie staining was used for detection. (c) Calibration of the NBD-PE lipid fluorescence intensity, used to deduce lipid yield of NBD-PE labeled liposomes.

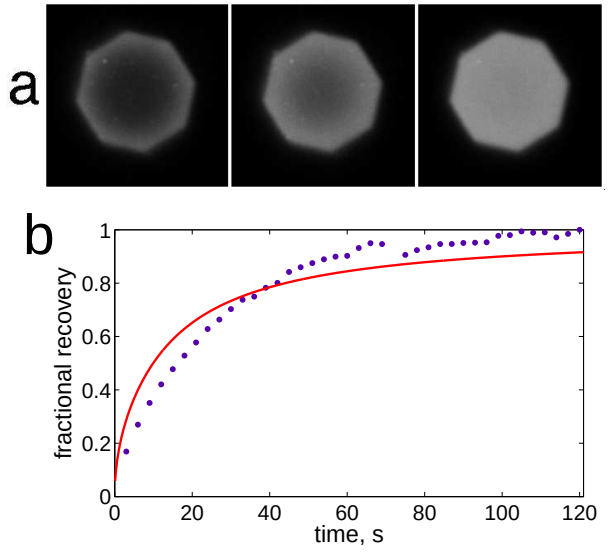

Figure S 2 A typical FRAP measurement before a v-SUV/t-SBL fusion test. (a) The SBL is doped with 2% NBD-PE, which is bleached only in the center of the viewfield by closing the field diaphragm to its minimum. The bleached region is $17\ \mu$m in diameter. The frames correspond to 3, 15 and 120 s after bleaching ended and recovery started. Recovery occurs due to flux of unbleached labeled lipids through the edges of the bleached zone. (b) Average fluorescence intensity in a circle that fills the bleached zone as a function of time (dots). The red curve is a fit to the data assuming a circular bleach zone at $t = 0$, full recovery, and negligible bleaching during read-out (eq. 3 of ref. 14), which yielded $D = 6.5\ \mu\text{m}^2/\text{s}$. This simple experiment does not fulfill all these assumptions, and consequently a perfect fit is not expected. The fit is only intended to get a rough estimate of the quality of the SBL before a fusion test with v-SUVs. T=32 $^\circ$C. Averaging measurements from 7 similar SBLs yielded $D = 6.28 \pm 0.54\ \mu\text{m}^2/\text{s}$ ($\pm$ s.e.m.).

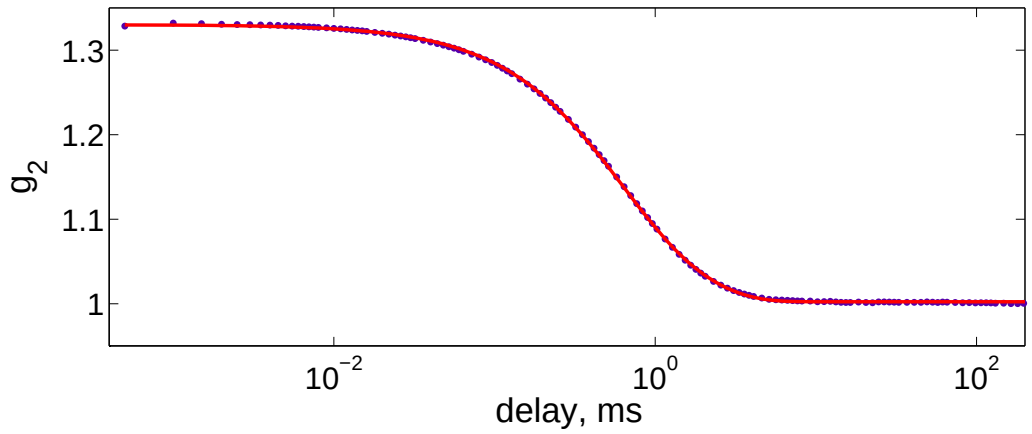

Figure S 3 Characterization of vesicle sizes by dynamic light scattering. A typical intensity autocorrelation measurement (blue dots) and eq. (1) fitted to data (red curve). The fit yielded the relaxation frequency $\overline{\nu} = 0.76$ /ms , relative variance $\delta = \mu_2/\overline{\nu}^2 = 0.37$, $B = 1.002$, and $\beta = 0.328$, implying $R_n \approx 29$ nm (see text). (v-SUVs, L:P=571, T=25 C, $R^2 = 1.00$.)

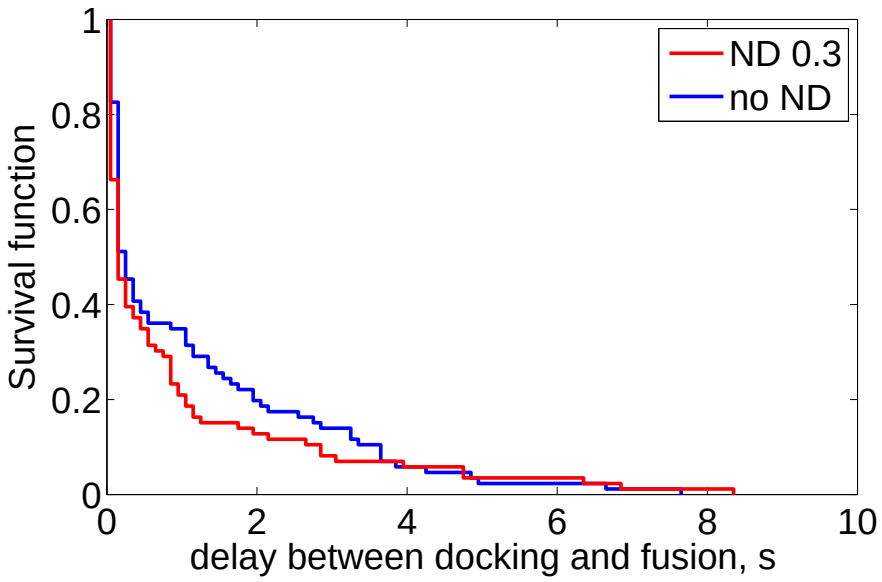

Figure S 4 Effect of incident light intensity on the distribution of delay times between docking and fusion. The data in blue are obtained without any neutral density (ND) filters, whereas a ND with an optical density of 0.3 (cutting 26% of incident intensity) was used for data in red, under otherwise identical conditions, from the same regions on a t-SBL (t-LP=10K, v-LP=120, 86 delays in each case). In other experiments wherein the incident light intensity was controlled by over a factor of ~ 4 by varying the aperture diaphragm also resulted in delay distributions that were indistinguishable within experimental error.

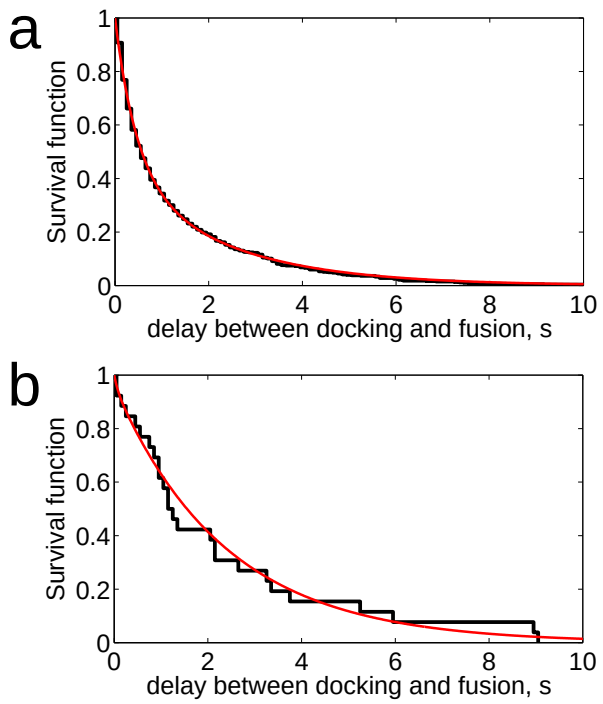

Figure S 5 Distributions of delay times between docking and fusion for t-SNARE and protein-free (pf) SBLs. (a) Delays for t-SBL/v-SUV fusions. A fit to the distribution using a mixture of two exponential decays of the form $a\exp(-t/\tau_1)+(1-a)\exp(-t/\tau_2)$ gave $a=0.57\pm0.06$, $\tau_1=0.46\pm0.06$ s, $\tau_2=2.26\pm0.23$ s. (t-L:P=10K, v-L:P=120, $n_{expt}=8$, $n_{fus}=605$) (b) Delays for fusions between pf-SBLs and the same v-SUV preparation as in (a) ($n_{expt}=8$, $n_{fus}=28$). The experiments in (a) and (b) were run in parallel. Only a single time scale is evident for pf-SBLs. A single exponential distribution model yielded $\tau=2.29\pm0.45$ s. Use of a mixture of two exponentials did not improve the confidence intervals returned by the fitting routine and led to a negligible amplitude for the fast component: $a=0.04\pm0.07$, $\tau_1=0.08\pm0.13$ s, $\tau_2=2.38\pm0.50$ s.

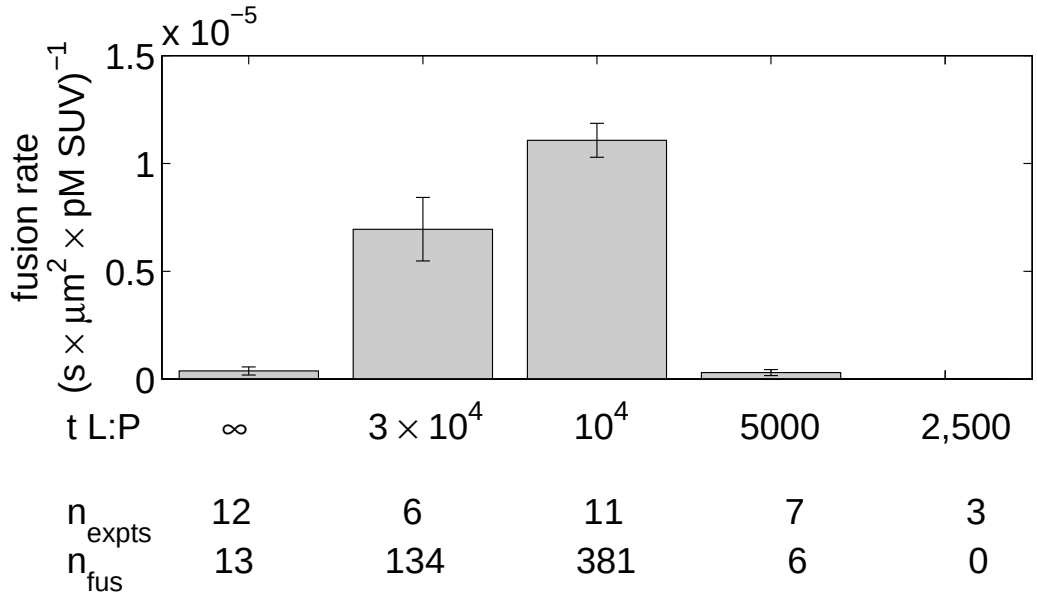

Figure S 6 The normalized fusion rate, $\dot{f}$, as a function of SBL t-SNARE lipid:protein ratio (t-L:P) measured at 32 $^{\circ}$C. The total number of single fusion events and the number of experiments are indicated for every t-L:P tested (v-L:P=150).

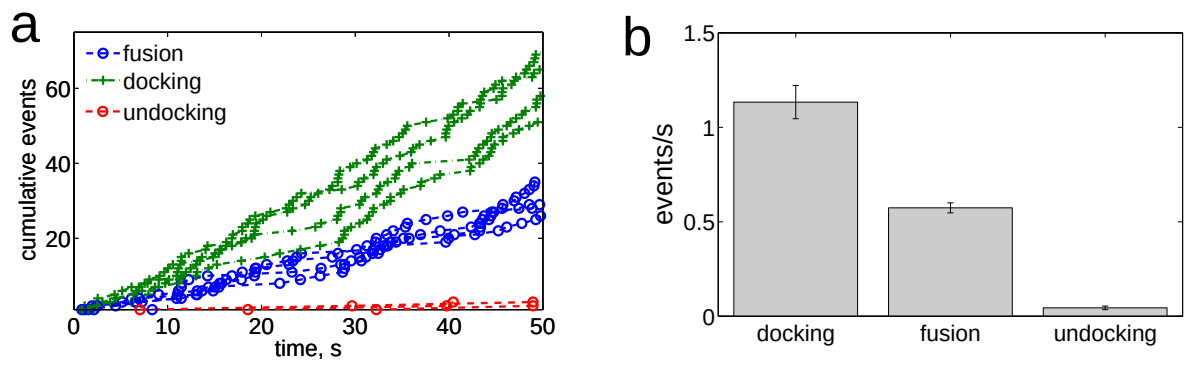

Figure S 7 Comparison of the rates of total docking, fusion and undocking rates. Total docking comprises all docking events, whether or not the docked vesicle fused. (a) Cumulative number of total docking, fusion, and undocking events as a function of time. (b) Average rates of (unnormalized) total docking, $\dot{D}_{tot}$, fusion, $\dot{F}$, and undocking, $\dot{U}$, obtained from the slopes of the plots of cumulative events in (a). The ratio of the fusion rate to the overall docking rate is 0.50, whereas $\dot{U}/\dot{D}_{tot} = 0.039$, implying ≈ 50 % and ≈ 4 % of the docked vesicles end up fusing or undocking, respectively (v-L:P=150, t-L:P=10,000, T=32 $^{\circ}$C). The acquision areas and SUV concentration were the same for all acquisitions in this set of data.

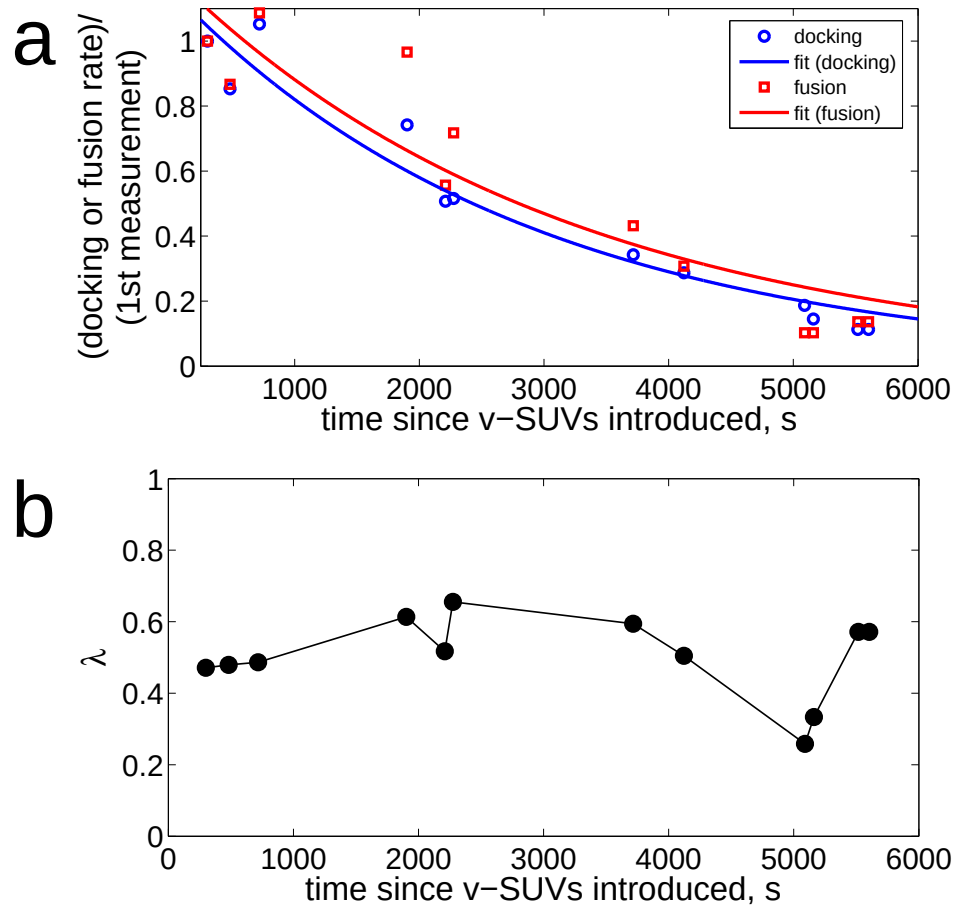

Figure S 8 The rates of fusion and total docking (counting all docking events regardless of the fate of the docked vesicles) as a function of time. (a) The rates of fusion (red squares) and total docking (blue circles) as a function of time, normalized to the value of the first measurement. Exponential fits to the data yielded: $a = 1.16 \pm 0.15$, $\nu = (3.46 \pm 0.78) \times 10^{-4}$ /s ($R^2 = 0.95$), $a = 1.21 \pm 0.25$, $\nu = (3.15 \pm 1.16) \times 10^{-4}$ /s ($R^2 = 0.85$) for the docking and the fusion rates, respectively. (b) The ratio, λ, of the fusion rate to the total docking rate as a function of time. The rate of total docking remained $\sim 2\times$ the rate of fusion.(t-L:P=10K, v-L:P=150, T=32 $^\circ$C.)

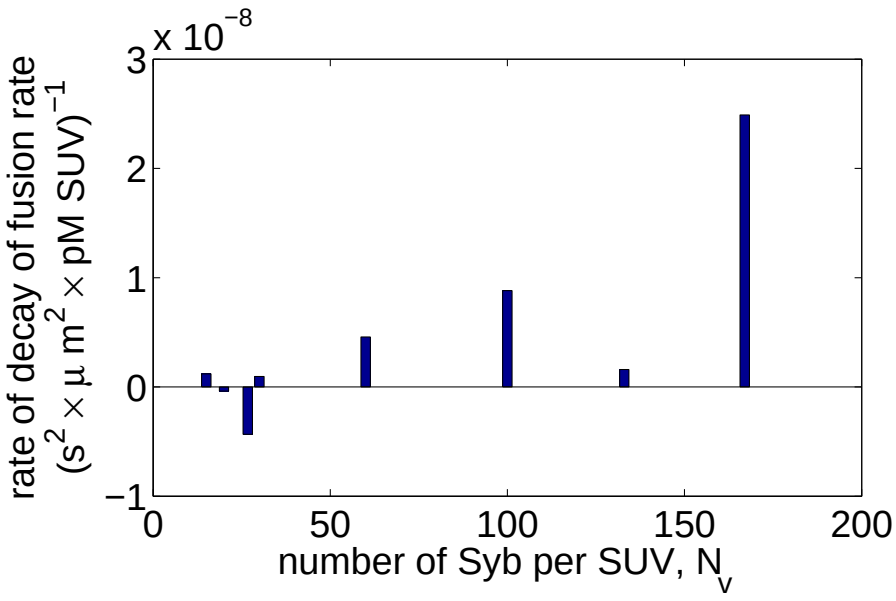

Figure S 9 The rate of decay of the fusion rate depends on the number of Syb per SUV, N_v. The higher N_v, the faster the rate at which the overall fusion rate $\dot{f}$ decreases. Below $N_v \approx 60$, the decay rate was too low to be detectable within a ≈ 2 hr period. (t-L:P=10K)

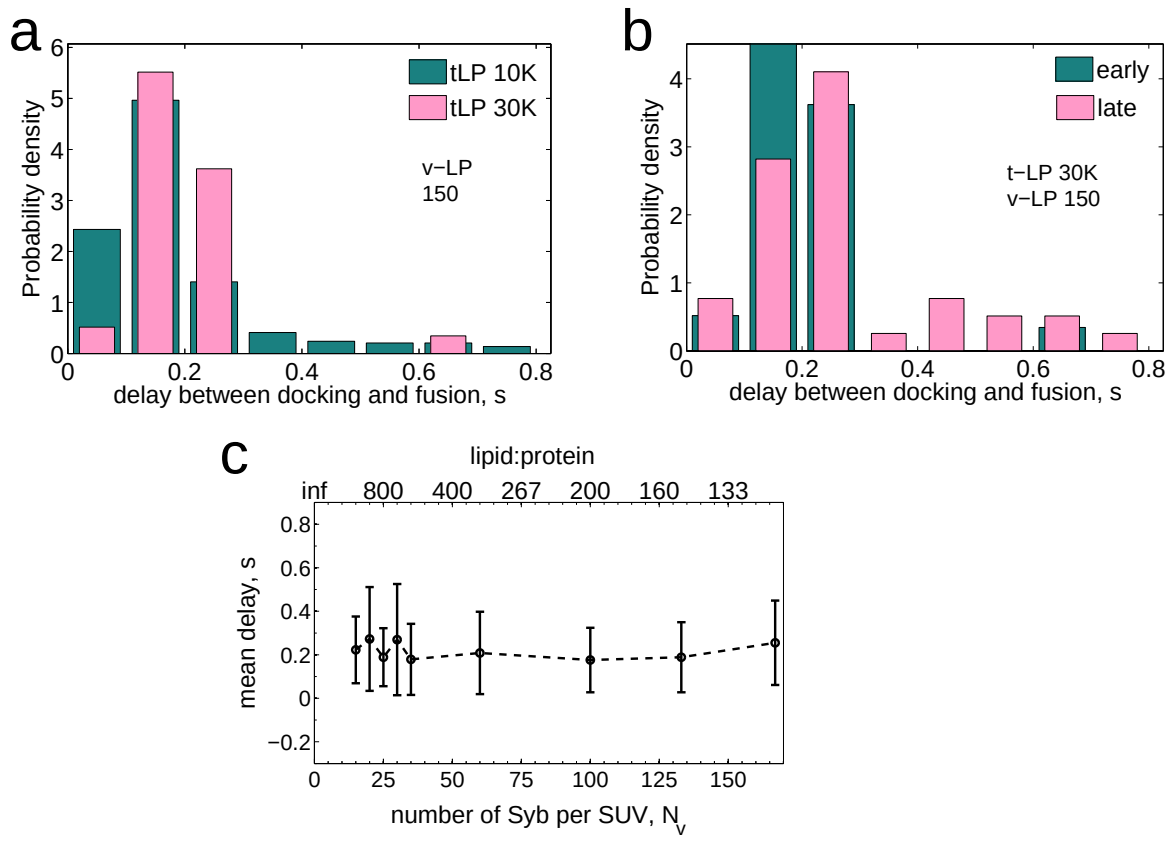

Figure S 10 Delays between docking and fusion are limited by recruitment of t-SNAREs. (a) Delays are longer for SBLs with lower t-SNARE densities (higher t-LP). The mean delays are 180 ms and 200 ms for SBLs with t-LP=10K and t-LP=30K, respectively. (b) Delays recorded within 30 min of v-SUV/t-SBL reactions ("early", mean=200 ms) are shorter than delays recorded at late times ($t > 2$ hrs) when t-SNAREs have been depleted ("late", mean=270 ms). (c) Mean delays as a function of N_v, the number of Syb per SUV.

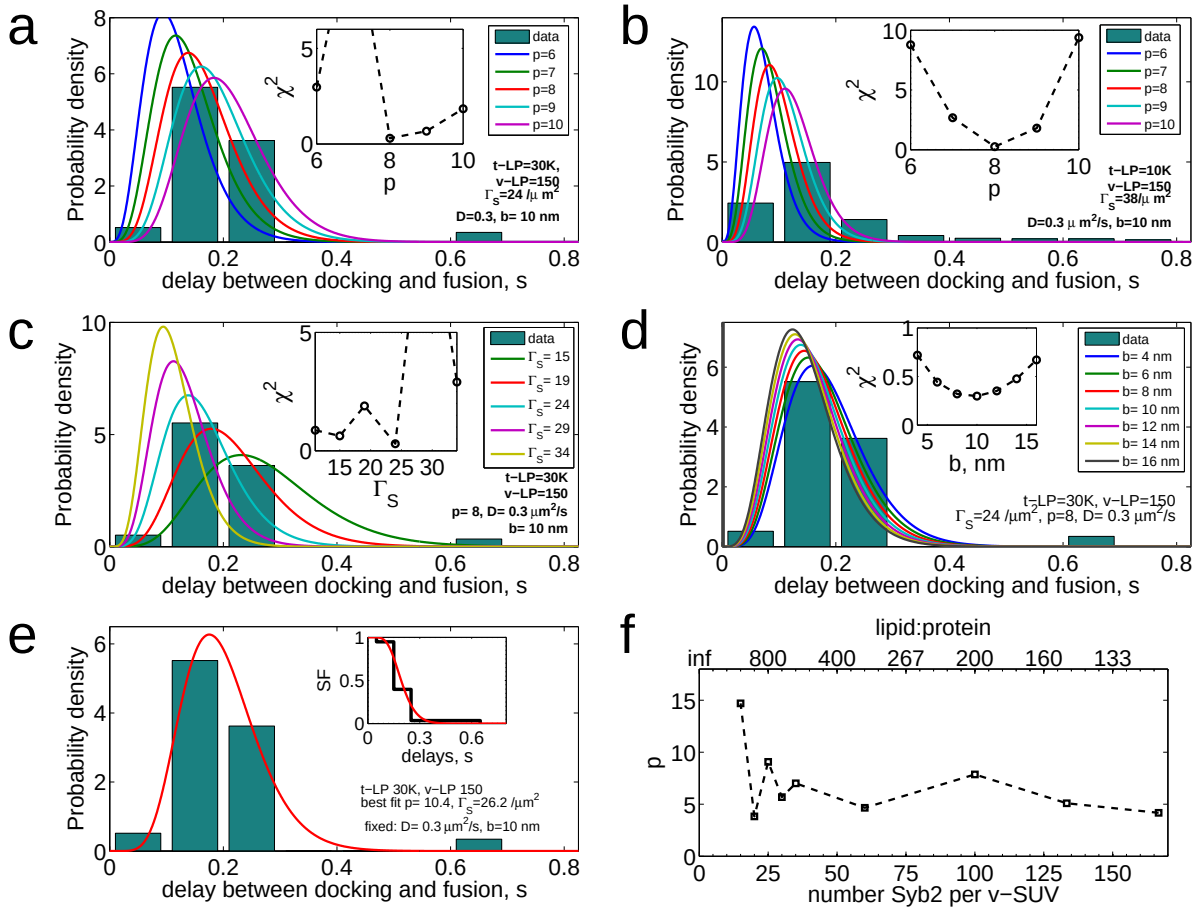

Figure S 11 Comparison between the SNARE recruitment model and measured delay distributions. (a) Theoretical curves calculated for the indicated p values, using D and Γ_S values based on measurements of ref. 11, and $b = 10$ nm. Inset: the χ^2 statistic measuring how close the theoretical curves are to the measured distribution. $p = 8$ is a global minimum. (b) Similar to (a), except for higher t-SNARE density (t-LP=10K). The SNARE density relative to data in (a) (t-LP=30 K) is estimated based on the relative overall fusion rates, $\dot{f}$ at the two t-LP values (see fig. S 6). Remarkably, $p = 8$ is again a global minimum for the χ^2 plot. (c) The effect of varying Γ_S. All other parameters were fixed as indicated. (d) The effect of varying the capture radius, b. The other parameters were fixed at the indicated values. (e) Allowing both p and Γ_S to be

free fitting parameters (for fixed D and b), for the same data as in (a) returned $p = 10$ and $\Gamma_S = 26$, remarkably close to the value of Γ_S based on measurements (*11*) and the p value found to give the closest match in (a). Inset: the empirical survivor function for the same data (black) and the corresponding fit (red) (f) Best fit p value found from fits such as in (e), as a function of N_v, the number of Syb per SUV. The average over N_v is $p = 6.9 \pm 3.4$ ($\pm$ std, 9 sets of experiments, 40-456 delays and 2-14 experiments per set, t-LP=10^4, 1,219 fusions in total).